## Werk

**Jahr:** 1981
**Kollektion:** fid.geo
**Signatur:** 8 Z NAT 2148:50
**Digitalisiert:** Niedersächsische Staats- und Universitätsbibliothek Göttingen
**Werk Id:** PPN1015067948_0050
**PURL:** http://resolver.sub.uni-goettingen.de/purl?PPN1015067948_0050

**LOG Id:** LOG_0015
**LOG Titel:** Geomagnetic induction studies in Scandinavia
**LOG Typ:** article

## Übergeordnetes Werk

**Werk Id:** PPN1015067948
**PURL:** http://resolver.sub.uni-goettingen.de/purl?PPN1015067948
**OPAC:** http://opac.sub.uni-goettingen.de/DB=1/PPN?PPN=1015067948



## Contact

Niedersächsische Staats- und Universitätsbibliothek Göttingen
Georg-August-Universität Göttingen
Platz der Göttinger Sieben 1
37073 Göttingen
Germany
Email: gdz@sub.uni-goettingen.de

J Geophys (1981) 50:23–36

Journal of Geophysics

# Geomagnetic Induction Studies in Scandinavia

## II. Geomagnetic Depth Sounding, Induction Vectors and Coast-Effect

Alan G. Jones

Institut für Geophysik der Universität Münster,
Gievenbecker Weg 61, D-4400 Münster, Federal Republic of Germany

**Abstract.** In this paper an event of very favourable structure for induction purposes, which was observed by the Scandinavian magnetometer array, is discussed and analysed in detail. The responses derived, in both the time and frequency domains, display a large coast effect at all coastal stations, both on the sea coasts and on the Gulf of Bothnia. Two relatively large inland anomalies are also delineated. The more significant of the two, the Storavan anomaly, is apparent using all the analysis techniques employed, and may be associated with a remnant of the Svionian island arc system. The less dominant anomaly, in the vicinity of Mieron, has no obvious correlation with geology or tectonic formations, and appears to be polarisation sensitive – it is only energised by east-west magnetic fields.

First approximation modelling of the coast effect observed by the northwestern stations illustrated that the responses are well satisfied by the conductivity contrast between sea and land.

Finally, the validity of the derived induction vectors, and the possible effects of induction for source field studies, are discussed.

**Key words:** Magnetometer arrays – Geomagnetic induction studies in Scandinavia – Coast effect – Geomagnetic depth sounding

### Introduction

In this work, the second of a series of papers (the first being Jones (1980), hereafter referred to as Paper I) concerned with various aspects of geomagnetic induction in Scandinavia as observed by the Münster IMS magnetometer array (Küppers et al. 1979), some qualitative aspects of the induced field, and a first approximation modelling of the coast effect, will be described.

Magnetometer array studies for induction purposes, using large numbers of variometers, mostly based on the original Gough-Reitzel design (Gough and Reitzel 1967), have been very successful in mapping the flow of anomalous electric current associated with lateral variations of electrical conductivity, either in the crust, or the upper mantle, or both. Reviews of some array studies, and techniques for analysing and presenting the data, are to be found in, for example, Gough (1973a, b), Frazer (1974) and Lilley (1975).

In almost all previous $2D$ magnetometer array studies, with the notable exception of that of Bannister and Gough (1977), the feature of prime interest was the Earth's internal conductivity structure. Thus, the magnetometers were typically 10–20 km apart, both to detect small scale anomalies and to avoid spatial aliasing problems. For the Scandinavian array however, the main purpose was the detection and analysis of local magnetic disturbance fields and their interpretation in terms of possible ionospheric current structure. Hence, the station spacing was of a minimum of some 80 km, and was typically 120 km, in northern Scandinavia, and of 200–300 km in southern Scandinavia. Such a spacing restricts an induction study utilising the data to only the gross effects observable.

In this paper an event, exhibiting an unusually uniform horizontal magnetic field, is described, and the data are analysed qualitatively, by various techniques, both in the time and frequency domains. The resulting information details two rather strong inland conductivity anomalies, and describes enhancements of the vertical magnetic field both at the sea coast and at the Gulf of Bothnia. The coast effect, as observed by the northwestern stations, is modelled by a thin sheet approximation, and it is shown that the data do not require a lateral variation in the crust and mantle between the ocean and the continent, although such a variation cannot be excluded.

### Data

The observations to be discussed in this paper were recorded by the Münster IMS Scandinavian Magnetometer Array (reported in Küppers et al. 1979) of modified Gough-Reitzel magnetometers (Gough and Reitzel 1967; Küppers and Post 1981) at the 24 locations shown in Fig. 1. All pertinent information regarding these stations is to be found in Table 1 of Küppers et al. (1979).

The particular interval chosen for this study was 13:00–16:00 UT on 6 July 1977, because of the somewhat unique characteristics of the magnetic field during this time. The three-component magnetic data from the 24 locations shown in Fig. 1 were digitised, reduced to variations relative to the quiet-time base line (taken as the field level during the interval 03:30–04:30 UT, also on 6 July 1977), and rotated into the Kiruna Cartesian coordinate system. This gave magnetic components, here labelled $x(t)$ (geomagnetic "north"), $y(t)$ (geomagnetic "east") and $z(t)$ (vertical, positive downwards) (note: in other papers dealing with data from this array the labels $A$, $B$, $Z$ have been employed to denote north, east, and vertical respectively), with a temporal resolution of 10 s, and a typical magnetic variation resolution of 2 nT (Küppers et al.

0340-062X/81/0050/0023/$02.80

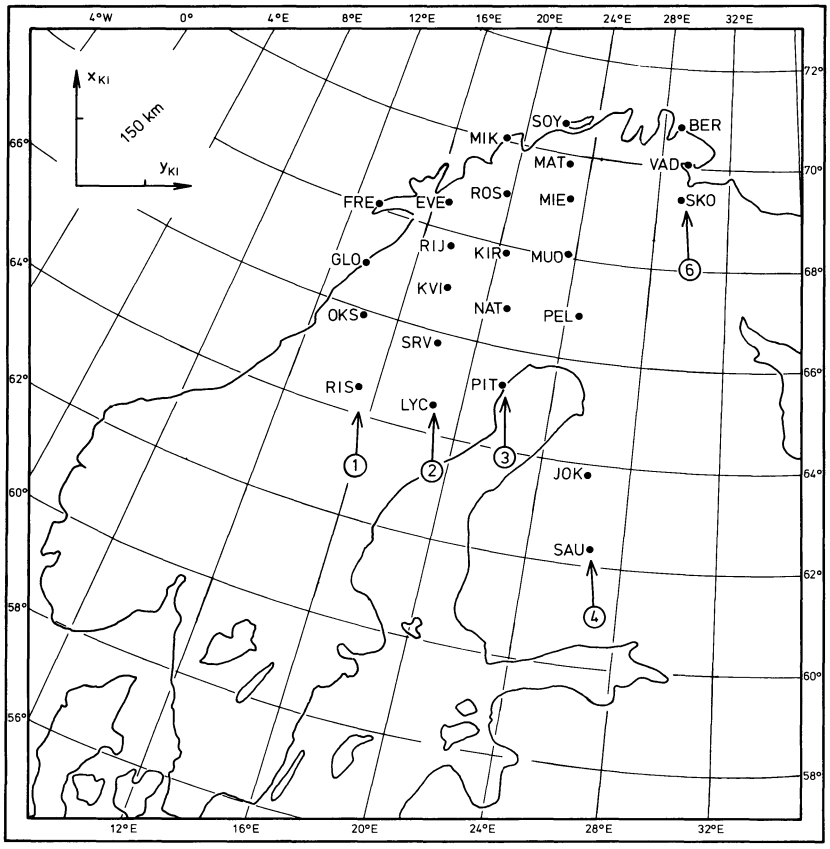


**Fig. 1.** Map showing the locations, in geographical co-ordinates, of the magnetometer stations which provided data for the event discussed in this study. In the upper left-hand corner are indicated the axes of the Kiruna cartesian co-ordinate system (see text). Profiles 1–4 and 6, which are perpendicular to lines of constant revised corrected geomagnetic latitude, are designated by the encircled numbers

1979, see also Jones, in press 1981a). The definitions of "north" and "east" for a particular location are given in Küppers et al. (1979). These data were chosen for analysis for induction purposes because of the large degree of horizontal field spatial uniformity that existed during the interval. The data are illustrated in Fig. 2 as profiles 1, 2, 3, 4, and 6 (Fig. 1) of the $x$, $y$, and $z$ components. The approximate spatial uniformity exhibited, which is seen in the horizontal components, is a very uncommon feature of magnetic data observed at these high geomagnetic latitudes.

## Information in the Time Domain

A simple inspection of the magnetograms recorded by an array of instruments often reveals the gross features of the lateral variations in conductivity. In particular, the component most indicative of internal conductivity inhomogeneities is the vertical magnetic field $z$. Large features are known to produce phase shifts, and even phase reversals, in $z$ between two points spanning an inhomogeneity. An excellent example of this simple method for mapping a large 2D feature is given by Alabi et al.'s (1975) work on the North American Central Plains (NACP) anomaly (see their Fig. 3).

No such gross effect as the NACP anomaly is observed in northern Scandinavia, but the data illustrated in Fig. 2 display the following characteristics:

(i) very strong attenuation of the high-frequency components of the $z$-field with distance away from the coast (Fig. 2), particularly for profiles 3, 4, and 6,
(ii) attenuation with decreasing latitude of the low-frequency components of the $z$-field,
(iii) re-emergence of high-frequency components in the $z$-field at stations SRV (profile 2) and PIT (profile 3, on the Gulf of Bothnia),
(iv) phase reversal in the high-frequency $z$-components observed along profile 3, with undetectably small high-frequency content at KIR,
(v) no phase shift observed over the whole array associated with the peak in the $x$-component at 14:00:00 UT,
(vi) strong increase in the $y$-component observed at OKS (profile 1) when compared with the neighbouring stations of GLO and RIS,
(vii) marked increase in the $y$-component at LYC (profile 2),
(viii) general attenuation in the $y$-component moving from the north-east (e.g., BER) towards the south-west,
(ix) attenuation in the high-frequency content in the $y$-component with distance away from station MUO (profile 4).

Because the data were reduced to variations relative to a quiet-time value (see above), and not to an arbitrary level, it is possible to derive the equivalent external current density for a particular instant of time. Figure 3a illustrates the approximate equivalent external current density on the ground, observed at 14:00:00 UT (corresponding to the peak in the $x$-component) over northern Scandinavia. The equivalent external current density, displayed as vectors at each station, was derived by taking the instantaneous magnetic disturbance vectors at 14:00:00 UT and estimating that the internal/external field ratio, given by $(1-kC)/(1+kC)$ (Schmucker 1970; 1973) with $k$ (source wavenumber) $\simeq 1/2000$ km (see below) and $C$ (inductive response function) $\simeq 130$ km (see Paper I, Table 1, period of 890 s), was $\simeq 0.9$. The thus estimated exter-

nal magnetic field on the ground was interpreted in terms of current density by assuming that a homogeneous current sheet of infinite extent flowed directly above the instrument, i.e., $(j_e)_y = 2(x_e)/\mu_0$. The magnetic field situation at 14:00:00 UT is representative of the general situation existing during the two "bursts" of activity, i.e., 13:40–14:20 UT and 15:15–15:45 UT. The high degree of spatial uniformity in the horizontal disturbance field is shown clearly. The corresponding vertical disturbance field, as contoured in Fig. 3b, as well as precisely describing a coast effect, also infers an inhomogeneity in the PIT-SRV-LYC region. It should be stressed here that any anomalous features observed in the vertical field must have their counterparts in the horizontal fields, hence *total* spatial uniformity of the horizontal fields is not possible. (Anomalies are however generally more difficult to detect in the horizontal components because, for a totally uniform field over a 1 D flat earth, the internally induced and externally inducing fields are of equal magnitude, but are opposite in phase in the vertical component, and in-phase in the horizontal components, leading to $z_t = 0$, $x_t = 2x_e$ and $y_t = 2y_e$, where subscript $t$ denotes total field components.) Latitude profiles in a co-ordinate system 20° anti-clockwise to the Kiruna system (corresponding to the direction shown by the KIR equivalent current vector), exhibit a strikingly longitudinally uniform N 20° W magnetic field with a latitudinal attenuation of $-0.065\,\mathrm{nT\,km^{-1}}$ (Fig. 4a). The horizontal magnetic component resolved in the direction N 70° E exhibits a longitudinal attenuation of approximately $-0.11\,\mathrm{nT\,km^{-1}}$ (Fig. 4b), but some non-uniform effects are apparent. These values of the spatial gradients of the horizontal fields, and the estimate of the inductive response function $C \simeq 130$ km, give an estimate of the normal vertical field, from

$$Z_n = C\left(\frac{\partial X}{\partial x} + \frac{\partial Y}{\partial y}\right)$$

(see, for example, Schmucker 1970; Jones 1980) of $z_n \simeq -25$ nT. The instantaneous vertical field exhibits this value in central northern Scandinavia, but at the northern coastal stations and towards the south-west and south strong non-1*D* earth effects are apparent.

It must be stressed that such a comparison between the horizontal and vertical fields at a particular instant of time may be used only in a qualitative manner and conclusions must be expressed tentatively. This is because the observed instantaneous fields are only related in a strict sense if the induction is purely in-phase. Out-of-phase components lead to time delays between the inducing and induced parts (Schmucker 1980; Jones in press 1981b).

The features described in this section can be split into two parts, those arising from the source-field, and those arising from the induced fields. Features (ii), (v), (viii) and Fig. 4a, b are all illustrative of the non-uniformity of the source field. The rest show effects of internal contributions which are certainly not insignificant.

## Information in the Frequency Domain

The spectral content of the event is illustrated by the sonogram analysis of the data from stations KIR (Fig. 5) and BER (Fig. 6). The data were recursion filtered by a narrow bandpass, with a selectivity of 0.3 (Hermance 1973), at centre periods of B1 = 60 s, B2 = 100 s, B3 = 200 s, B4 = 300 s, B5 = 450 s, B6 = 600 s and B7 = 1,000 s. The data exhibit the features that (i) there is no information below 100 s, (ii) at 100 s there are only data in the first interval of activity, i.e., 13:30–14:30, (iii) the polarisation characteristics of the first and second intervals of activity (i.e., 13:30–14:30 and 15:00–16:00) are different at all periods, and (iv) the approximate spatial uniformity of the horizontal field is observed over the whole frequency range. The latter two points are especially important when estimates of response functions are to be determined, as will be discussed later.

Estimates of the smoothed auto-spectral densities (or "power spectra") for each component, and of the cross-spectral densities between pairs of components, were derived by the usual techniques of statistical frequency analysis. The steps involved were:

(i) extraction of all data in the interval 13:01:00–15:51:40 UT to give a reduced data length of 1,024 points per component,
(ii) removal from each component of zero, first and second order polynomial trends,
(iii) application of a cosine taper to the first and last 10% of each component data series,
(iv) computation of the raw Fourier spectra, of 511 complex and 2 real harmonics, of each component,
(v) first-order correction of the instrument response, as illustrated in Küppers and Post (1981), by multiplying each harmonic with the term

$$1 + i\frac{\omega_c}{\omega},$$

where $\omega_c$ is the $-3$ dB point of the component response curve. The response of a typical instrument fitted reasonably well to a first-order low-pass Butterworth filter with $-3$ dB points given by: $x$-component = 9·5 s; $y$-component = 13·0 s; and $z$-component = 5·5 s,
(vi) computation of raw auto and cross spectra,
(vii) smoothing of raw auto and cross-spectra by a constant $-Q$ box-car window, with $Q = 0.3$ ($Q = \Delta\omega/\omega_0$),
(viii) normalising the smoothed spectra by data set length, and by the factor 1/0.875 to correct for the application of the cosine taper (Bendat and Piersol 1971), to yield $\hat{S}_{ab}(\bar{\omega})$, the estimated cross spectra between components $a(t)$ and $b(t)$.

### *Fourier Spectra Maps*

Contouring of Fourier spectra at a certain period has proved in past array studies to be a useful technique for delineating conductivity anomalies (see de Beer and Gough 1980 and references therein). Indeed, in a recent work Gough and de Beer (1980) consider that Fourier spectra maps are superior to induction vector information when the horizontal components are strongly interdependent (see discussion on this topic in later section).

For this event of 3 h duration, the longest period at which stable spectral estimates can be made is of the order of 1,000 s, due to spectral frequency smoothing considerations which are necessary in order to reduce the associated variance of the estimates. The maps chosen for illustration are those at 1,000 s, for reasons detailed below, but they are representative of the range 200 s–1,000 s.

It was found that the contoured maps of the real and imaginary parts of the smoothed Fourier spectra gave more detail than did the more usual maps of amplitude and phase. Figure 7a–f show the real and imaginary parts of the three

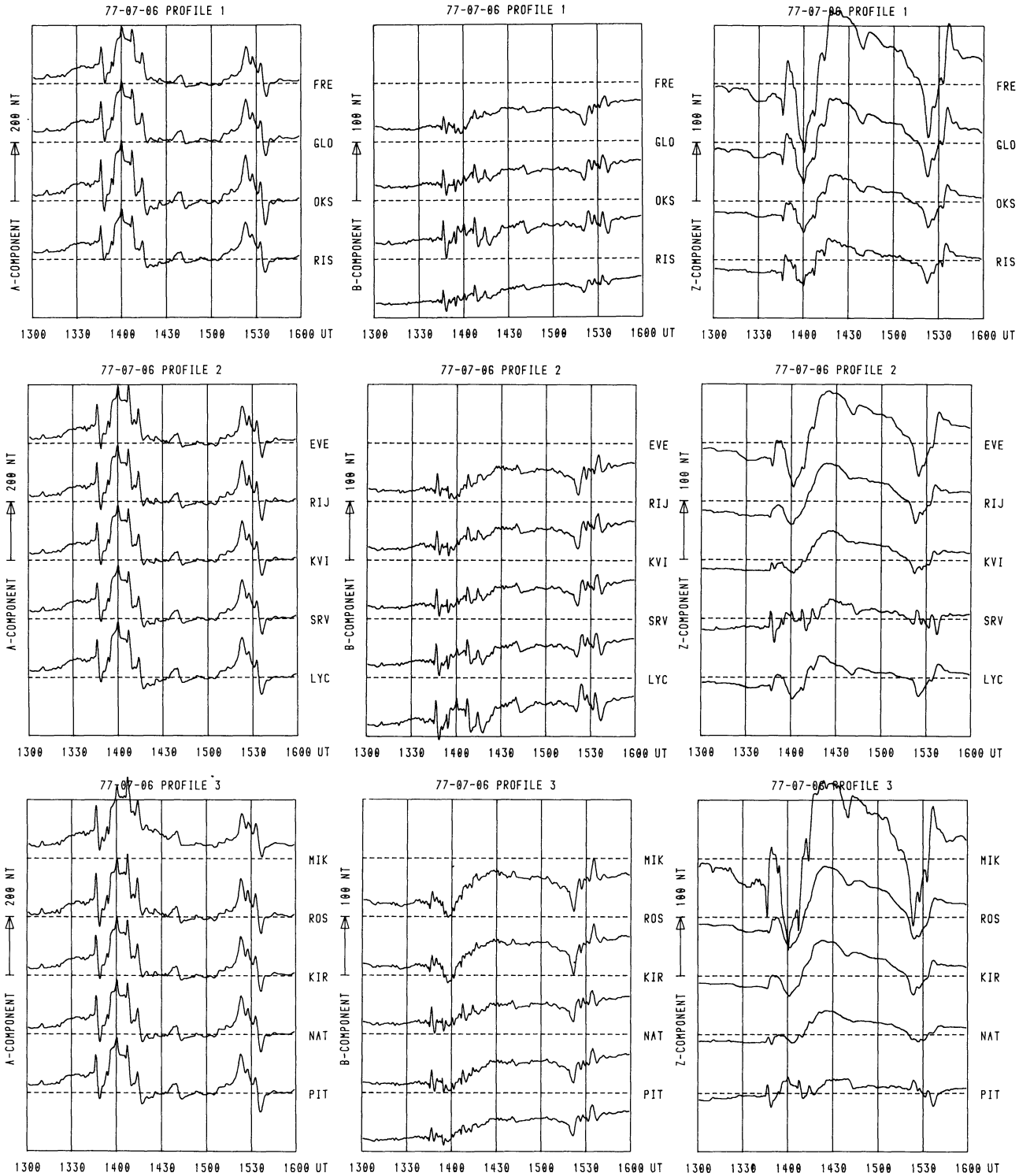


**Fig. 2.** Magnetic disturbances, as recorded by the stations illustrated in Fig. 1, in the interval 13:00–16:00 UT on 6 July 1977, compared with quiet-time baselines (*dotted lines*). *A*, *B*, and *Z* components refer to north, east, and vertical respectively in the Kiruna co-ordinate system (note: these components are termed $x(t)$, $y(t)$ and $z(t)$ in the text). The data are stacked along Profiles; *Profile 1* FRE→RIS; *Profile 2* EVE→LYC; *Profile 3* MIK→PIT; *Profile 4* SOY→SAU; *Profile 6* BER→SKO

components at 1,000 s period. The polarisation characteristics are shown in Fig. 9a and correspond to an average field over the event as observed at KIR with a major axis pointing due north, an ellipticity of 0.12, and a ratio of polarised power to total power of 0.98. That the event displays an almost linear polarisation is regarded as advantageous for Fourier spectra mapping from the conclusions drawn by Gough and de Beer (1980).

Figure 7a–f confirm the major details already seen in the data as set out above, namely:

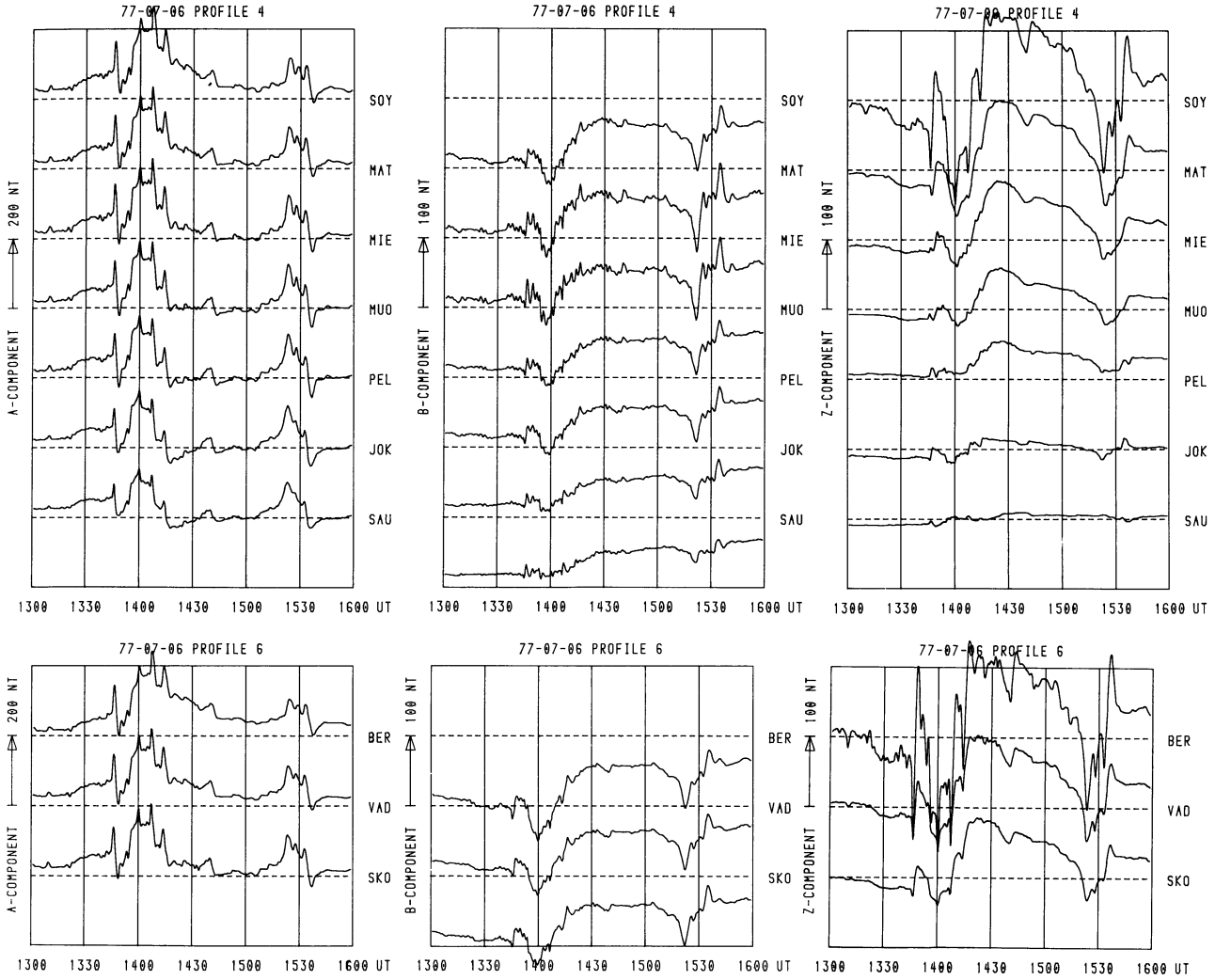


point (iii), the Storavan anomaly (Im($Y$), Re($Z$) and Im($Z$)), point (ix), the Mieron anomaly (Re($Y$), Im($Y$) and Re($Z$)), and point (i) a strong coast effect (Im($Z$)).

Amplitude and phase maps (not shown here) confirm the comments by de Beer and Gough (1980) that the intracontinental anomalies are best seen in the *Z phase*, whilst the coast effect shows in *Z amplitude*.

*Polarisation Characteristics of the Horizontal Field*

Any two-component vector field may theoretically be decomposed into three parts: (i) totally polarised signal, (ii) totally unpolarised signal, and (iii) noise contributions (Jones 1979). However, without an *a priori* knowledge of the noise terms, such a decomposition is not possible and the expressions detailed in Fowler et al. (1967) may lead to biased estimates of the polarisation parameters (Jones 1979).

Figure 8a, b illustrate the auto-spectral densities of the three-magnetic components for stations KIR (Fig. 8a) and BER (Fig. 8b). The greatest noise contribution is believed to be the digitising error (Jones in press 1981b) of the order of 2 nT, the level of which is indicated by the broken line at 15 $nT^2$ $Hz^{-1}$, i.e., the power spectral density level of a 1068 point random series, of variance 2.75 nT, extended by zeroes to 2048 points. As described by Fig. 8a, b, the power spectra exhibit a very strong attenuation with decreasing period, with the result that the signal-to-noise ratio of the horizontal components only becomes insignificantly small at periods less than about 100 s. Hence the polarisation parameter estimates will not be significantly biased at periods greater than 100 s.

The polarisation parameters were derived from the smoothed auto- and cross-spectra by the expressions given in Born and Wolf (1964) (repeated in Fowler et al. 1967 and Jones 1979). The polarised parts of the fields observed at each location are illustrated as ellipses at four periods; 1,000 s, 450 s, 200 s and 100 s in Fig. 9a–d respectively. The ratio of polarised power to total power was mostly in the range 0.90–0.95 at all stations for periods greater than 100 s. In the polarisation maps, the strong uniformity of the horizontal field is again evident, but other features can also be seen. The general decrease in ellipticity at 1,000 s and 450 s going from the NE to SW is a function of the decreasing $Y$ field in this direction, and hence is a source effect. However, the following are not explainable by source contributions:

(i) the increase in polarised power with distance away from the coast along profiles 2, 3, and 4 at all periods,

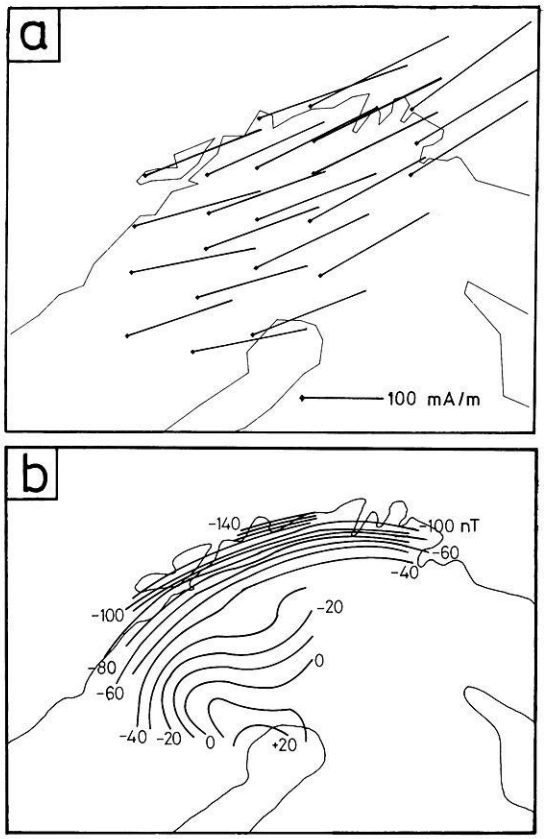


**Fig. 3. a** Upper panel: Equivalent external current density, as observed by the magnetometer array, at 14:00:00 UT on 7th July 1977; **b** Lower panel: the vertical magnetic disturbance field on the ground for the same time instance as Fig. 3a

(ii) the tendency for the ellipse observed at LYC to be orientated more to the east than at SRV and KVI, also on profile 2,
(iii) the small polarised power observed at RIS at all periods compared with neighbouring stations.

*Induction Vector Information*

The single-station transfer functions $[T_x, T_y]$ are defined as those functions that minimise, in some sense, the error of the fit to the equation

$$Z = T_x X + T_y Y + \xi \tag{1}$$

(dependance on frequency assumed throughout), which relates the vertical magnetic field component to the horizontal magnetic field components at the same frequency. It is obvious that for any fields whatsoever transfer functions $[T_x, T_y]$ may be estimated. What is of paramount significance is whether the derived functions may be interpreted in terms of induction effects. The assumptions under which such an interpretation is valid are:

(i) $Z \sim Z_a$, i.e., the vertical field contains approximately no normal part,
(ii) $E[S_{z_n x}] = E[S_{z_n y}] = 0$ (where E denotes expectation value), i.e., the horizontal fields do not correlate with any normal vertical field,
(iii) $X \sim X_n$, $Y \sim Y_n$, i.e., the horizontal fields can be approximated to be normal.

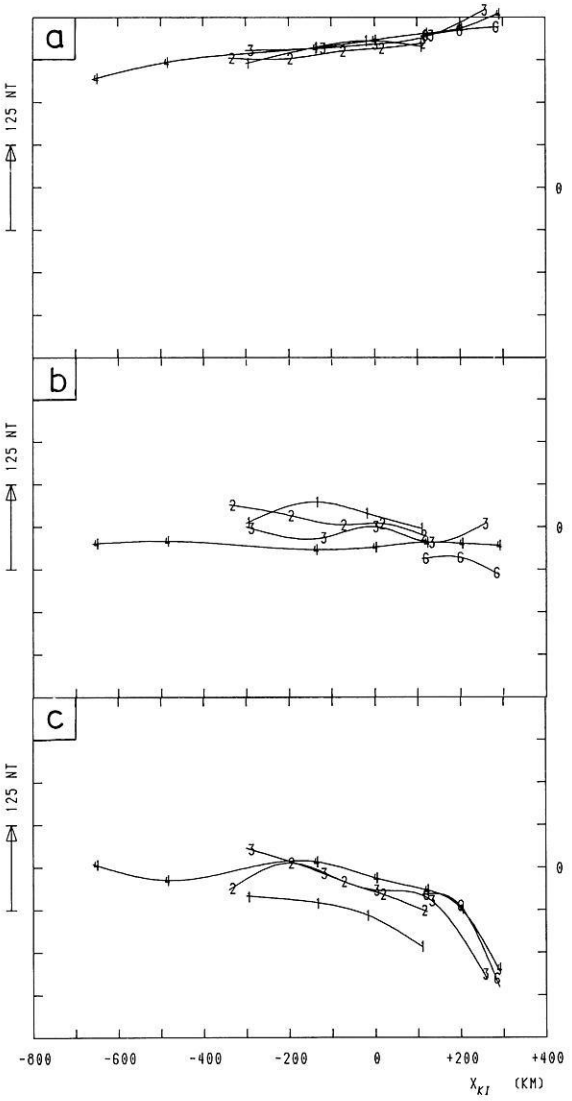


**Fig. 4a–c.** Latitudinal profiles at 14:00:00 UT on 7 July 1977 in the rotated co-ordinate system, given by a 20° anti-clockwise rotation of the Kiruna co-ordinate system, i.e., such that the magnetic disturbance field observed at Kiruna (KIR) (see Fig. 3a) has no eastward or westward directed component in the rotated system. **a** Upper panel; northward directed magnetic disturbance field along profiles 1 to 4 and 6, as denoted by the numbers; **b** Middle panel; eastward directed magnetic disturbance field; **c** Lower panel; vertical magnetic disturbance field

Furthermore, a $2D$ interpretation of the observed $[\hat{T}_x, \hat{T}_y]$ tacitly assumes that current channelling effects, due to $3D$ conductivity structure, are not significant.

The most widely used expressions for estimating $[T_x, T_y]$ are those which lead to estimates unbiased by noise contributions in $X$ and $Y$ (Jones in press 1981a). This estimate for, for example, the $T_x$ transfer function is

$$\hat{T}_x = \frac{\hat{S}_{xz}\hat{S}_{yy} - \hat{S}_{xy}\hat{S}_{yz}}{\hat{S}_{xx}\hat{S}_{yy} - \hat{S}_{xy}\hat{S}_{yx}}. \tag{2}$$

The denominator of Eq. (2), which may be written as $\hat{S}_{xx}\hat{S}_{yy}(1-\hat{\gamma}^2_{xy})$, where $\hat{\gamma}^2_{xy}$ is the estimated coherence between components $x(t)$ and $y(t)$, indicates the well-known requirement that $x(t)$ and $y(t)$ must contain some independent information, i.e., that the horizontal field is not totally polarised.

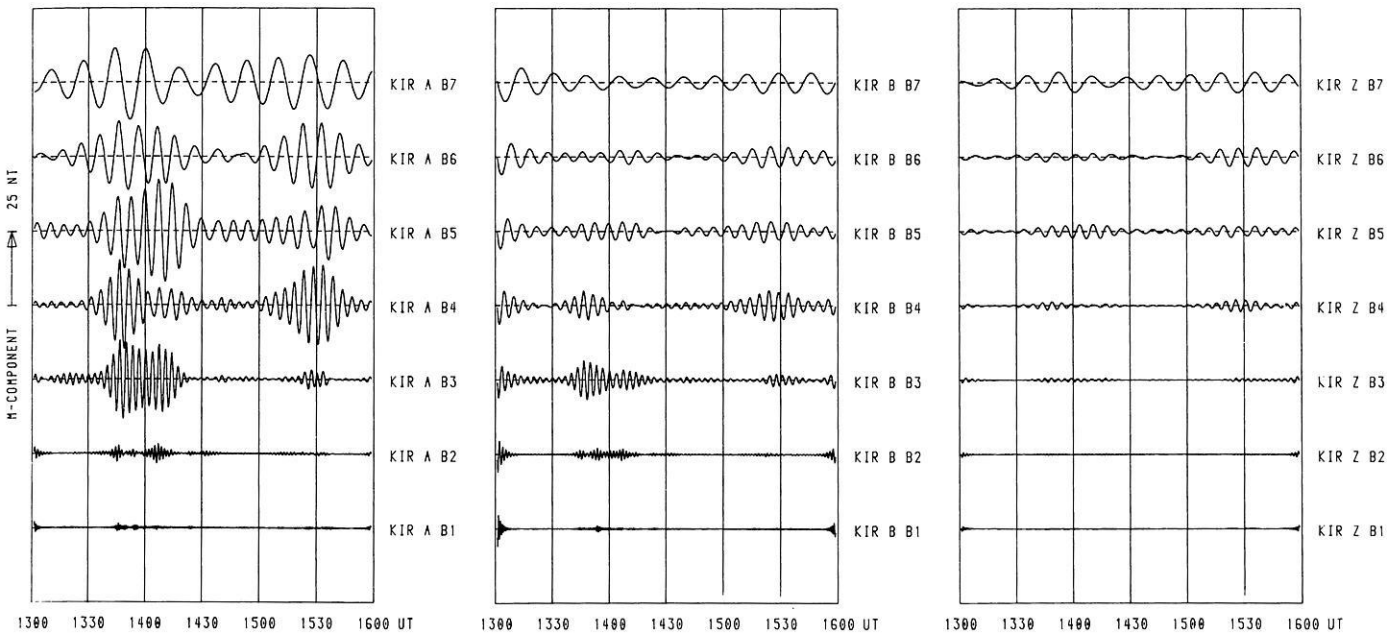


**Fig. 5.** Sonogram analysis of the magnetic disturbance recorded at Kiruna (KIR - see Fig. 1). The filters had a selectivity of 0.3, and a centre period of: B1 60 s; B2 100 s; B3 200 s; B4 300 s; B5 450 s; B6 600 s; B7 1,000 s ($A, B, Z$ as in Fig. 2)

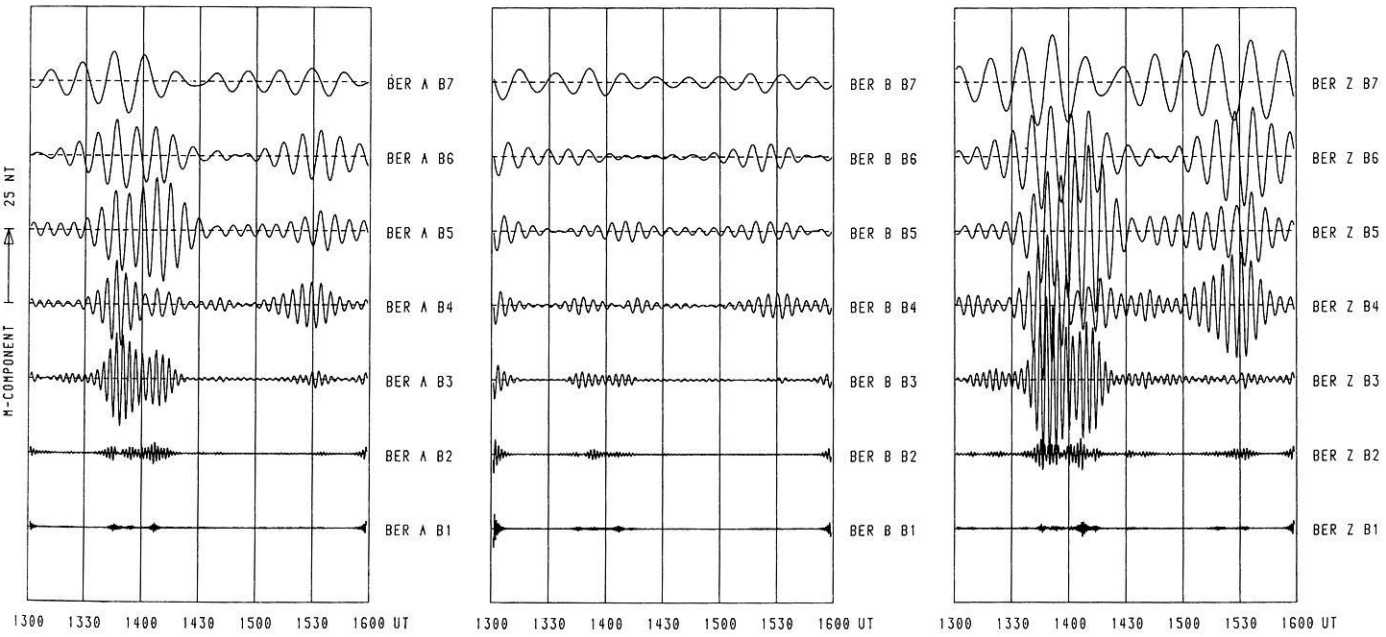


**Fig. 6.** As Fig. 5 but for the data recorded at Berlevag (BER - see Fig. 1)

A quantitative measure of how well the estimation process has been undertaken is given by the estimates of the circles of confidence, at a certain probability level, applicable to the estimates $[\hat{T}_x, \hat{T}_y]$. Assuming that the error, $\xi$, in Eq. 1 is a random variable with a normal probability distribution function and which is totally uncorrelated to $x(t)$, $y(t)$, or $z(t)$, the estimates of the radii of the circles of confidence are given by

$$\hat{r}_x^2 = \frac{4}{\nu - 4} F_{4;\nu-4;\alpha} \frac{(1-\hat{\gamma}_{zxy}^2)}{(1-\hat{\gamma}_{xy}^2)} \frac{\hat{S}_{zz}}{\hat{S}_{xx}} \tag{3}$$

(similarly for $\hat{r}_y^2$ by replacing $\hat{S}_{xx}$ with $\hat{S}_{yy}$)

where

$\nu$ = number of degrees of freedom associated with the estimate, given by twice the number of raw estimates averaged over ($\nu = 10$ at 1,000 s, and $\nu \simeq 100$ at 100 s)

$F_{4;\nu-4;\alpha} = 100\alpha$ percentage point of the $F_{4;\nu-4}$ distribution function,

and

$\hat{\gamma}_{zxy}^2$ = estimate of the multiple coherence between $z(t)$, and $x(t)$ and $y(t)$ as inputs, which is equal to $(1 - S_{\xi\xi}/S_{zz})$ (Goodman 1965, repeated in Bendat and Piersol 1971).

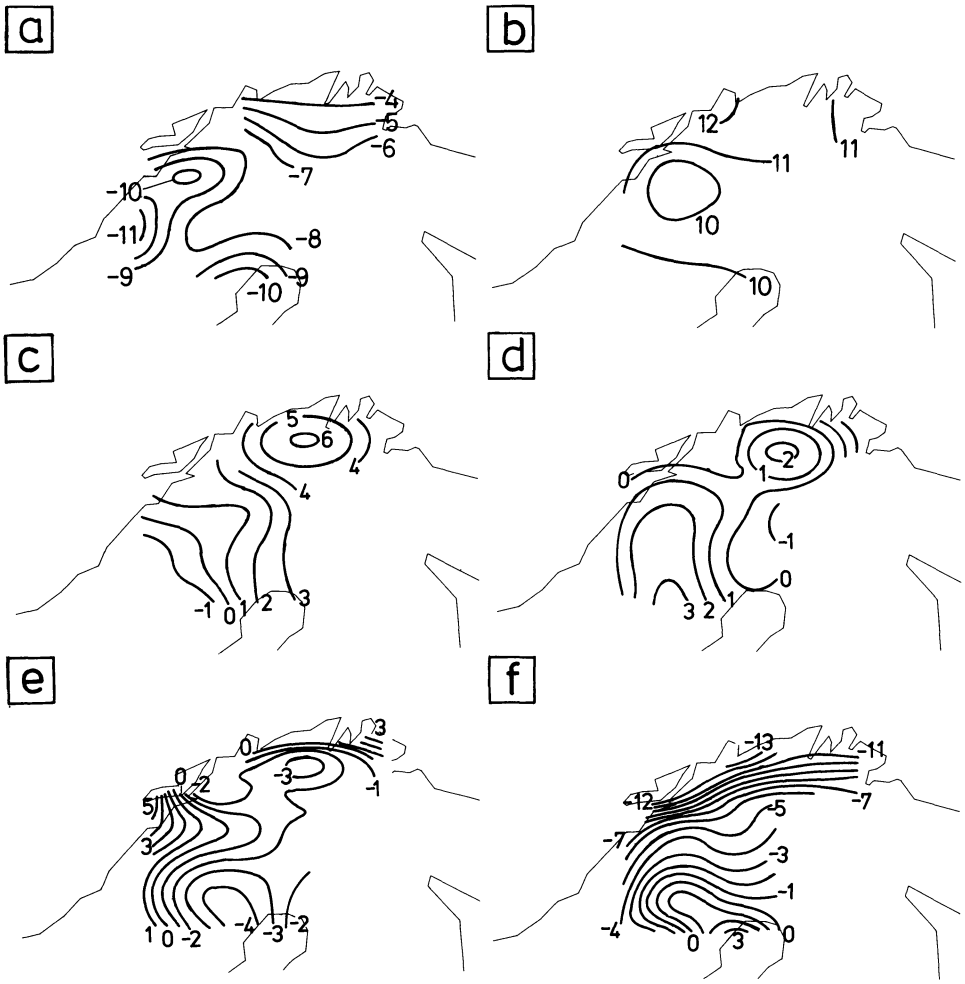


**Fig. 7a–f.** Smoothed Fourier spectral density maps for a central period of 1,000 s for the data illustrated in Fig. 2. **a** Upper left, real part of $X(f)$; **b** Upper right, imaginary part of $X(f)$; **c** Middle left, real part of $Y(f)$; **d** Middle right; imaginary part of $Y(f)$; **e** Lower left, real part of $Z(f)$; **f** Lower right, imaginary part of $Z(f)$ (arbitrary units)

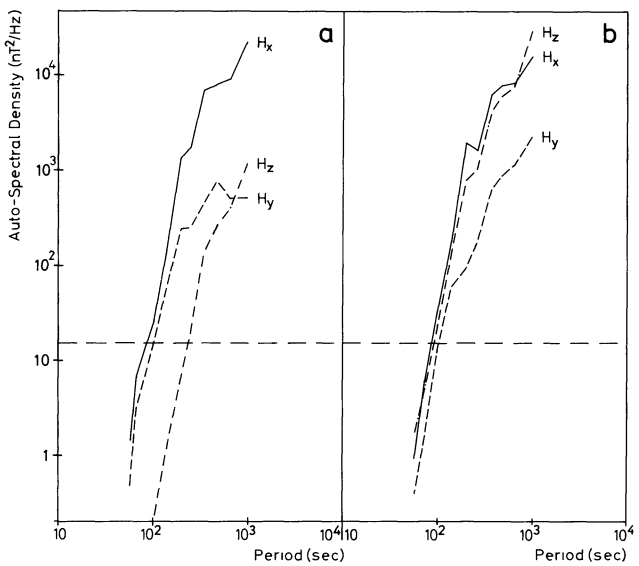


**Fig. 8a, b.** Smoothed Auto-Spectral Densities, in $nT^2/Hz$, for the data recorded at **a** KIR and **b** BER. $H_x$, $H_y$ and $H_z$ refer to the north, east, and vertical components respectively in the Kiruna system. The dotted line indicates the assessed resolution level (see text)

Denoting unit vectors **i** and **j** as pointing along axes $x_{KI}$ and $y_{KI}$ respectively, the estimated real and imaginary induction vectors are given from the estimates $[\hat{T}_x, \hat{T}_y]$ by

$$\hat{\mathbf{V}}_r = -\mathrm{Re}(\hat{T}_x)\ \mathbf{i} - \mathrm{Re}(\hat{T}_y)\cdot\mathbf{j} \tag{4a}$$

$$\hat{\mathbf{V}}_i = \mathrm{Im}(\hat{T}_x)\cdot\mathbf{i} + \mathrm{Im}(\hat{T}_y)\cdot\mathbf{j} \tag{4b}$$

(note that the real vector only has been reversed to point towards internal current), and the confidence intervals of $\hat{\mathbf{V}}_r$ and $\hat{\mathbf{V}}_i$ are described by an ellipse with axes $\hat{r}_x$ and $\hat{r}_y$.

The single-station induction vectors, estimated by Eqs. (2), (4a) and (4b) for the event, are illustrated in Fig. 10 (real) and 11 (imaginary) at the four periods 100 s (10a, 11a), 200 s (10b, 11b), 450 s (10c, 11c) and 1,000 s (10d, 11c). The 68% probability level confidence ellipses for the end points of each vector are also illustrated in the figures by their major (here $\hat{r}_y$ because of the smaller magnitude of $\hat{S}_{yy}$ compared with $\hat{S}_{xx}$; Fig. 8) and minor ($\hat{r}_x$) axes.

The coast effect is a very dominant feature of the derived in-phase induction vectors, but intracontinental effects are also noticeable:

(i) the small induction vector in the neighbourhood of KIR at 100 s–450 s,

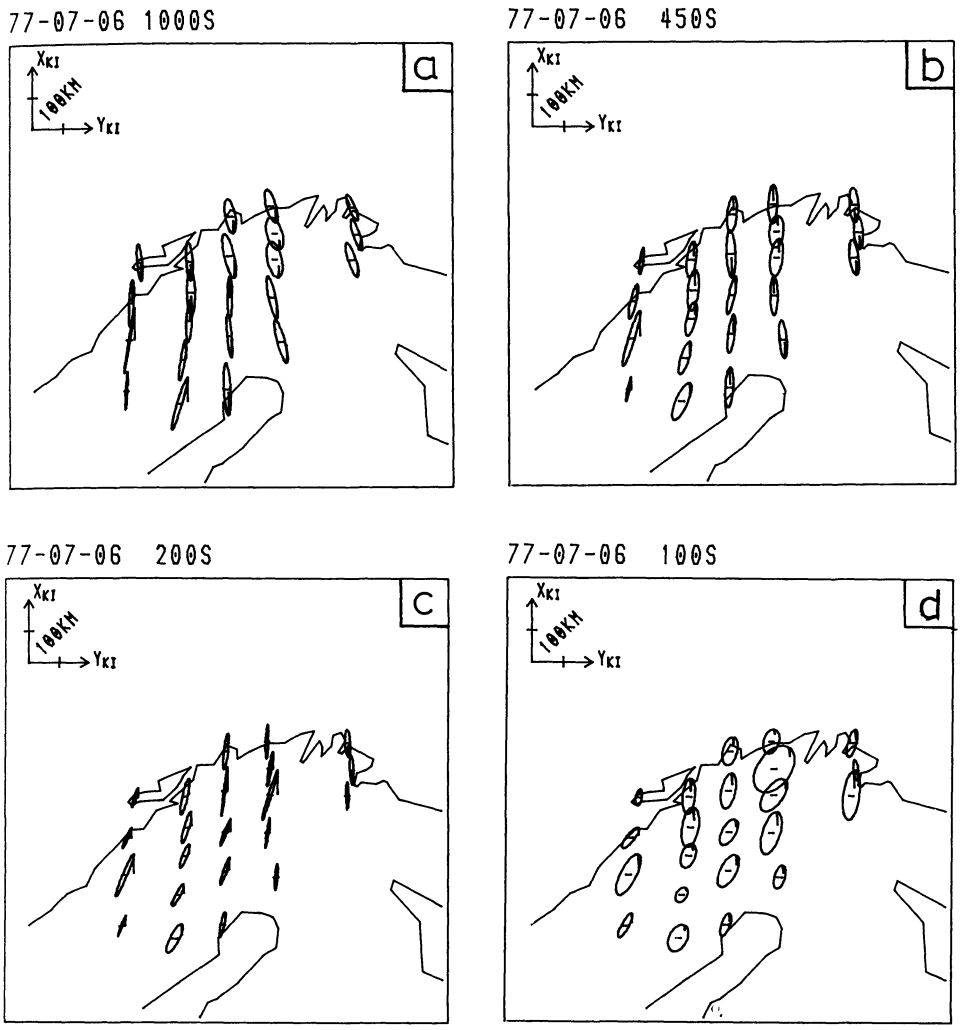


**Fig. 9a–d.** Ellipses of the polarised power of the horizontal magnetic field, as observed at **a** 1,000 s, **b** 450 s, **c** 200 s and **d** 100 s

(ii) the presence of a large anomaly in the OKS-RIS-SRV region,
(iii) the effect on the vectors at LYC and PIT due to the Gulf of Bothnia.

The large predominantly northward-pointing in-phase vectors observed at 1,000 s may be due to source-field influence. If KIR can be assumed to be over a horizontally layered earth, as concluded in Paper I, then the activity in the $z$-component at long periods ($>500$ s), as seen in Figs. 5 and 8, is an indication that the external vertical magnetic field is not being cancelled by the internally induced vertical magnetic field. Hence at long periods the source field of this event is not totally uniform. Work on 3 $D$ source fields over a 1 $D$ earth (Mareschal 1980) showed that data recorded further than 6° to 8° south of a 3 $D$ electrojet's southern boarder, the earth being a half space of 1,000 Ωm resistivity, will not be significantly affected for periods less than 60 min. However the very noticeable three-dimensionality of Scandinavia and the coastal and nearby oceanic waters make inferences of the induction effects of non-uniform source fields very difficult, but it may be concluded that even if source fields do affect the northern coastal stations, the effect is not significant for stations at geomagnetic latitude around that of OKS-PEL.

### Coast Effect

The coast around Scandinavia is, as illustrated in the bathymetry map (Fig. 12), of highly complex form. The Norwegian Sea is of deep ocean depths (2–3 km) and the continental edge is close to the Lofoten station of FRE, but the Barents Sea is shallow, less than 500 m, for the most part less than 300 m, over its whole extent.

In order to examine the coast effect exhibited along a line perpendicular to the continental edge (AA′ in Fig. 12), the estimated single-station transfer functions $[\hat{T}_x, \hat{T}_y]$ were rotated into a co-ordinate system with axes parallel and perpendicular to the coast, to yield $[\hat{T}_{\parallel}, \hat{T}_{\perp}]$. For the $E$-polarisation case, i.e., electrical current flowing SW/NE in the ocean, the ratio of the vertical to horizontal magnetic field is given by the transfer function $\hat{T}_{\perp}$.

The estimated real parts of the $\hat{T}_{\perp}$ transfer function at two periods, 200 s and 1,000 s, for stations FRE, GLO, EVE, ROS, RIJ, KVI, KIR, NAT, together with their associated 68% probability confidence intervals (i.e., one standard deviation of the mean) resolved into a direction parallel to AA′, are shown in Fig. 13. The station EVE exhibits a negative real part at 200 s, which may be an indication of current perturbation in Ofotfjord, a 60 km long fjord south of EVE (Evanes) leading to the port of Narvik. The negative $\mathrm{Re}(T_{\perp})$ observed at NAT is interpreted as due to current perturbation in the Baltic and around the Gulf of Bothnia (see next section).

A first approximation to the expected attenuation of the vertical/perpendicular-horizontal magnetic field ratio is given by the $E$-polarisation results of the somewhat drastic model

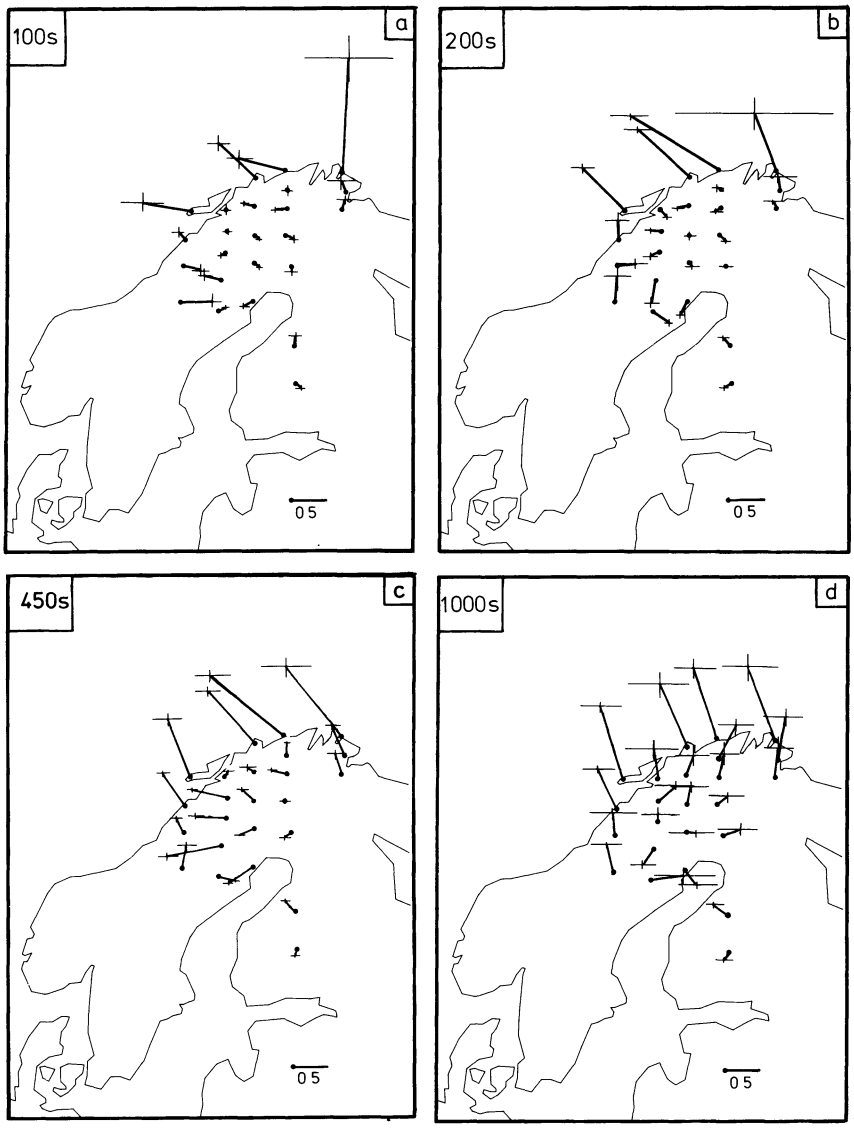


**Fig. 10a–d.** Reversed real induction vectors, and their 68 % intervals, as observed for periods of **a** 100 s, **b** 200 s, **c** 450 s, and **d** 1,000 s

of Fischer et al. (1978, reviewed in Fischer 1979) of a perfectly conducting ocean lying on a medium of uniform resistivity $\rho$. With the values of $\rho = 230\,\Omega$m at 200 s, and $\rho = 130\,\Omega$m at 1,000 s (taken from Paper I), the attenuation of $\mathrm{Re}(T_\perp)$ with distance from the ocean-land boundary was determined from Fig. 13 of Fischer (1979). This theoretical attenuation is displayed in Fig. 13, at the two periods, and a reasonably good fit to the data is achieved.

The effect of a laterally-varying integrated conductivity thin-sheet model, shown in Fig. 14, which describes the bathymetry (shown as a dashed line in Fig. 14) observed along profile AA′, with a subsurface of a 125 Ωm, 110 km thick layer overlying a 3 Ωm half-space (taken from Paper I), was calculated using the programme of Schmucker (1971). Two models were employed, one with, and one without, a "tau" representation of Vestfjord which lies between the Lofoten Islands and the mainland.

The derived $\mathrm{Re}(H_z/H_\perp)$ for both models are also illustrated in Fig. 13a, b, where a very good fit is apparent between the data and the model. At the shorter period GLO fits to the model without a Vestfjord, as should be expected as Glomfjord (GLO) lies directly on the coast, but it is clear that the data from RIJ and ROS are better explained by including an inductive effect in Vestfjord.

A very important conclusion to be drawn from this model fitting is that the data resolved along profile AA′ are almost totally explainable by induction at a coast-land boundary. No lateral variation in mantle conductivity along AA′ is required, although such a variation cannot be excluded.

The data along profile BB′, however, do not fit a much simpler $\tau$ model of

$$\tau = \begin{cases} 1{,}200\,\mathrm{S} & \text{for } 150\,\mathrm{km} < x \\ 1{,}000\,\mathrm{S} & \text{for } 0 < x < 150\,\mathrm{km} \\ 0.1\,\mathrm{S} & \text{for } x < 0, \end{cases}$$

where station BER is located at $x = 0$, to represent the shallow Barents Sea, over a three-layer substructure with parameters $\rho_1 = 10^4\,\Omega$m, $d_1 = 30$ km, $\rho_2 = 125\,\Omega$m, $d_2 = 140$ km and $\rho_3 = 3\,\Omega$m (model taken from Paper I). The values of $\mathrm{Re}(\hat{T}_x)$ are all a factor of 2–4 too large, which is interpreted as the influence of one, or both, of two possible effects:

(i) two-dimensional current flow around the northern coast of Scandinavia, in particular around the Varangerhalvöya penin-

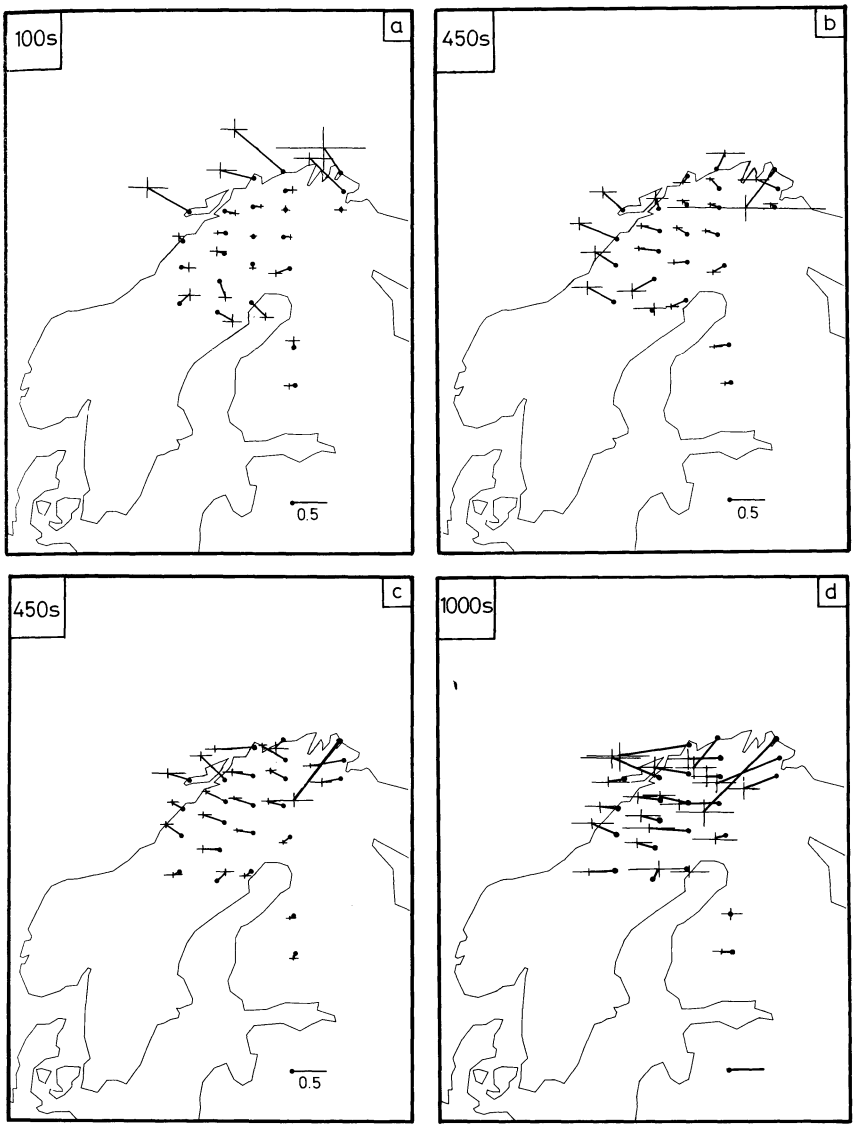


**Fig. 11a–d.** Unreversed imaginary induction vectors, and their 68 % confidence intervals, as observed for periods of **a** 100 s, **b** 200 s, **c** 450 s and **d** 1,000 s

sula on which Berlevag (BER) and Vadsö (VAD) lie,
(ii) distant source contributions, as discussed above.

The effect cannot be due to a more conducting mantle under the Barents Sea because, as shown by Dosso (1973), a conducting mantle under an ocean reduces the $H_z/H_x$ ratio.

## Discussion and Effects on Source-Field Studies

This paper has concentrated on an analysis, by many different methods, of one single event which was very suitable for induction purposes. The striking horizontal component uniformity, unusual for auroral and sub-auroral zones, ensured that particularly the variations in the vertical component, $z(t)$, reflected contributions from induced fields.

Two inland anomalies were identified in almost all of techniques employed on the data. The more dominant of the two, the Storavan anomaly, is delineated approximately by the stations PIT-LYC-OKS-SRV. This anomaly, which lies between the well-known Svecokarelian fault to the north (which in Finland is a zone of extensive mineralisation) and the Bothnian basin to the south, coincides almost exactly with a postulated remnant of the Svionian island arc systen (Meissner 1979). The other inland anomaly, the Mieron anomaly, which appears to be polarisation sensitive, does not correlate with any known geological or tectonic formation.

With respect to induction vectors and their determination, Gough and de Beer (1980) recently cast aspersions regarding the validity of interpreting induction vectors estimated from events where the horizontal components are clearly well correlated. Their study illustrated that vectors derived from one set of data - in this case their 1971 array data - do not agree with those from another set of data - their 1977 array data. They explained the discrepancy as being due to an incorrect choice of data for induction vector estimation purposes in the latter case, and suggested two "practical precautions"; (a) "events should have dissimilar $X$ and $Y$ magnetograms", and (b) "cross-correlations should be computed" (between the $X$ and $Y$ data) ... (and) "Events should be included whose cross-correlations peak at time shifts distributed between large positive and negative values". These constraints can however be easily deduced from inspection of Eq. (3), which gives the expression for estimating the confidence intervals of estimated transfer functions, and are already part of the theory of

statistical frequency analysis. For a two-input/single-output linear system, as described by Eq. (1), the confidence intervals are reduced by: (i) increasing $\nu$, the number of degrees of freedom, (ii) reducing $\hat{\gamma}^2_{xy}$, the estimate of the coherence between the two input series, i.e., $x(t)$ and $y(t)$, and (iii) increasing $\hat{\gamma}^2_{zxy}$, the estimate of the multiple coherence between the output, i.e., $z(t)$, and the two inputs. Point (i) may be accomplished either by ensemble averaging, i.e., over different realisations, or events, of the data, or by frequency smoothing, i.e., averaging together, in some fashion, a certain number of neighbouring raw Fourier harmonic estimates, or by both.

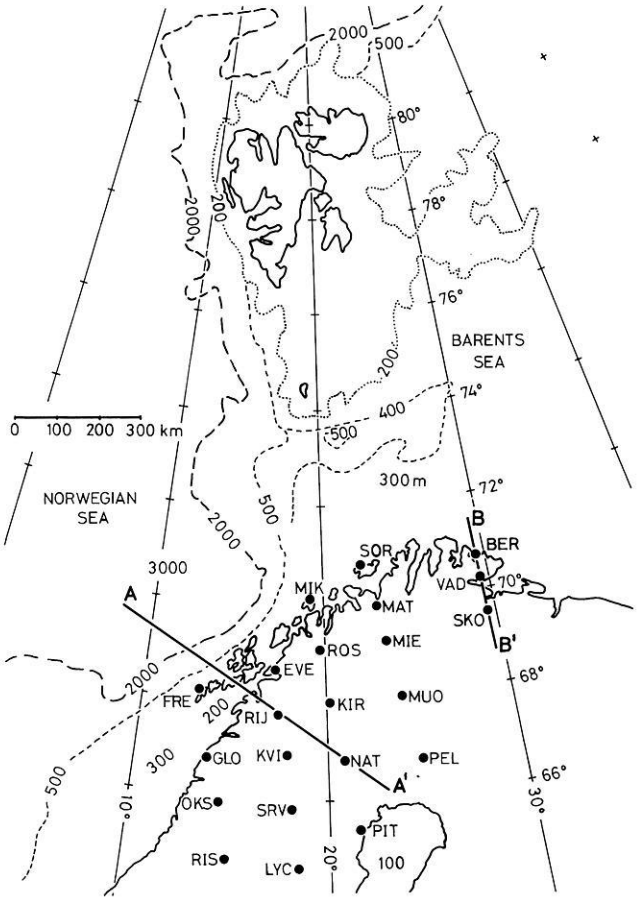


**Fig. 12.** Bathymetry map of the coast around northern Scandinavia, showing water depth (in meters), the station locations, and profiles AA′ and BB′

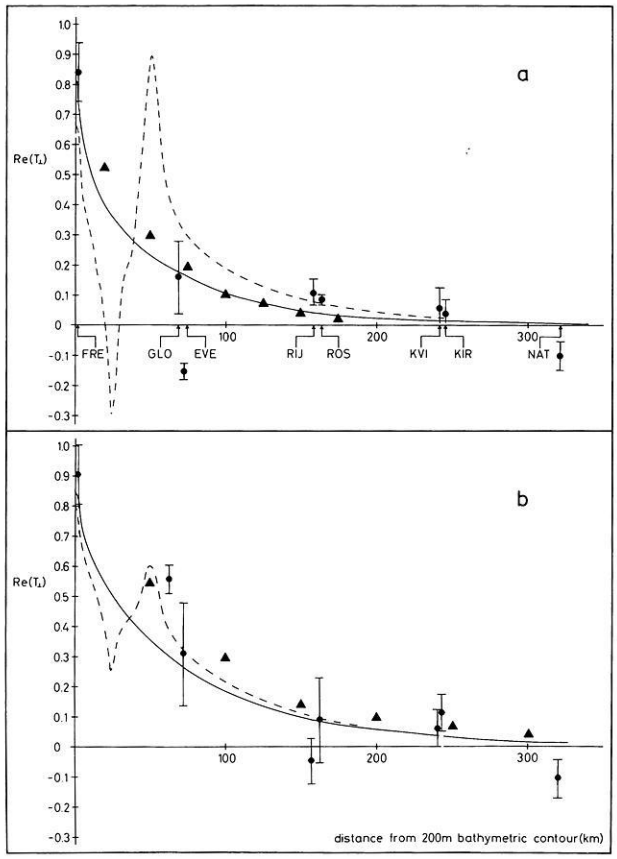


**Fig. 13a, b.** *Dots* indicate the magnitude of the real part of the inductive transfer function at **a** 200 s and **b** 1,000 s in the direction parallel to AA′, i.e., perpendicular to the coast, or *E*-polarisation, for the stations FRE, GLO, EVE, RIJ, ROS, KVI, KIR, and NAT, as compared to the distance from the 200 m bathymetric contour west of FRE (see Fig. 12). The ranges are the 68 % confidence intervals of the rotated functions. *Triangles* indicate the Fischer first-approximation of a perfectly conducting thin sheet overlying a half space at **a** 200 s and **b** 1,000 s for half-spaces of 230 Ωm and 130 Ωm respectively. *Full lines* are the Schmucker thin-sheet modelling results for the model shown in Fig. 14 without a Vestfjord representation. *Dashed lines* are the Schmucker thin-sheet modelling results for the model shown in Fig. 14 with a tau representation of Vestfjord (see text)

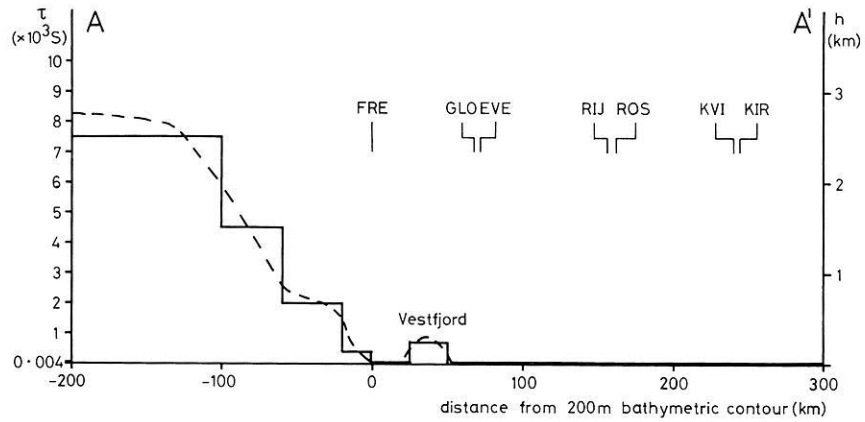


**Fig. 14.** *Full line:* thin-sheet model approximation of the lateral variation in crustal conductivity along Profile AA′. The continental crust has an integrated conductivity of 4 S. The locations of the stations, as resolved along AA′, are also illustrated. The thin-sheet surface overlies a 110 km thick layer of 125 Ωm, followed by a half-space of 3 Ωm. *Dashed line*: the variation in bathymetry along profile AA′. The position of Vestfjord, which lies between the Lofoten Islands and the mainland, i.e., between FRE and GLO, is also indicated

When performing such an operation however, it must be without doubt that $\nu$ is actually being increased, i.e., that the different individual estimates to be averaged contain independent information. For geomagnetic data, this requires that the source field structure be sufficiently different for each realisation, which is clearly not the case for 7 of the 10 events from the 1977 array data discussed by Gough and de Beer (1980), as shown by their Fig. 7 (lower part). Point (ii) above, the requirement of a low coherence between the two horizontal components, is a statistical description of point (b) of Gough and de Beer. The necessity of a high coherence, or correlation in the time domain, between $z(t)$ and the horizontal components, $x(t)$ and $y(t)$, is not mentioned by Gough and de Beer, but is obviously of equal importance to their points (a) and (b). For the 10 events from their 1977 array data, the ensemble average had a low $\nu$ (possibly only 3 significantly different polarisations from the 10 employed, see their Fig. 7, lower part) and a high $\hat{\gamma}^2_{xy}$, which both add to produce large values of the estimates of the confidence inervals of $[\hat{T}_x, \hat{T}_y]$, i.e., $\hat{r}^2_x$ and $\hat{r}^2_y$. It is therefore highly probable that, contrary to the statements of Gough and de Beer (1980), the vectors derived from the 1977 array data are totally in accord with those estimated from the 1971 array data.

For the event analysed here, the differing polarisations for the two "bursts" of activity, and at differing frequencies, ensured that the estimates would contain sufficient information. Also, by calculating the confidence intervals it is possible to be certain that, at the 68% confidence level, the directions and amplitudes are significant.

A first approximation modelling of the response function, observed along a line which is normal to the continental shelf structure, inferred that the data from stations FRE, GLO, EVE, RIJ, ROS, KVI, and KIR may be adequately explained by the conductivity contrast between the continent and the ocean. No lateral variation in lower crust or mantle conductivity was required. However, this does not exclude such a variation, it would be necessary to consider longer period variations, i.e., $>1$ h, to gain more insight into the likely variation of the Moho or asthenosphere at the continent – ocean boundary.

For the original purpose of the array, it is obviously of paramount importance if the coast effect and the two inland anomalies detailed herein have a significant effect on the total magnetic fields observed, as this would make untenable the rather direct interpretation of the magnetic disturbance vectors, as equivalent current vectors, usually undertaken by the Münster IMS group. As $3\,D$ Earth-conductivity modelling with typical ionospheric source structure has not yet been accomplished, the only recourse is to inspect work, either published or in press, for indications of effects that could be attributable to anomalous conductivity structures. The large positive time-difference $Z$ fields observed by PIT and MIK at the time of the abrupt "switch-on" of an additional current system, as detailed in Untiedt et al. (1978), Fig. 14, is possibly due to a phase delay of short period $Z$ variations, as inferred by the large imaginary induction vectors at short periods (see Fig. 11). The large negative $Z$ fields observed by stations MAT and MIE at 17:42 UT in Fig. 3 of Mersmann et al. (1979), when compared with the neighbouring stations of ROS and TR (Tromsö magnetic observatory), are possibly artifacts of the polarisation sensitive anomaly centered on those stations. In the same figure, the equivalent current arrows at PIT and OUL (Oulu, not shown here, see Fig. 2 of Küppers et al. 1979) are anomalous, and are due to induction in the Gulf of Bothnia region. This effect is also seen in Fig. 11 of Baumjohann et al. (1980) and Fig. 4 of Baumjohann and Kamide (in press 1981).

In the majority of cases, however, the influence of the induced parts is difficult to recognise or assess. It may not be in significant that the position of the differential $Z$-field minimum shown in Fig. 9 of Opgenoorth et al. (1980) corresponds exactly with the location of the Storavan anomaly, or that the maximum of the $Y$-field at 04:00–04:20 UT of the pulsation event of Glaßmeier (1980), Fig. 5b, is centered on stations MAT and MIE. Indeed, Glaßmeier noted that the polarisation characteristics of station MIE were ambiguous (his Fig. 7, 04:10 UT).

That the Mieron anomaly was not detected in the $2\,D$ field separations along profile 4 undertaken by Mersmann et al. (1979) and Küppers et al. (1979) is due to the polarisation properties of the anomaly. Both studies analysed data from $2\,D$ eastward electrojets, and, as has been shown, the anomaly becomes apparent only when there is a significant north/south component of equivalent current flow.

For source-field studies, the area of central northern Scandinavia is particularly free of inhomogeneities, hence permitting a $1\,D$ Earth approximation. A relevant model for this area is given in Jones (in press 1981c), and comprises a top layer of $10^4\,\Omega$m and 7 km thick (the sialic layer) overlying a moderately resistive lower crust of $360\,\Omega$m down to the Moho at 46 km, with a mantle of $80\,\Omega$m and an asthenospheric layer between 170–230 km depth of $5\,\Omega$m. For this model, at a frequency of $10^4$ s for a source field of wavelength 1,200 km, the ratio of the external field to the total field is 0.93, with a phase lead of the former of 140 s. Thus, the assumption made in Baumjohann and Kamide (in press 1981) of neglecting internal contributions for their study is justifiable for central northern Scandinavia to within 10%, which is the accuracy of the modelling involved (Baumjohann, private communication). For events of longer wavelength, or shorter period, the internal contributions become more significant. These comments are, it must be stressed, for a $1\,D$ Earth Contributions from a real earth, with especial regard to the coast effect, are expected to be larger. For example, over the Norwegian Sea (modelled by assuming a 2 km deep sea, of $\rho = 0.33\,\Omega$m, overlying a 5 km thick sialic layer, of $\rho = 10^4\,\Omega$m, over the same lower crust and upper mantle as above), the ratio of the external field to the total field at $10^4$ s period for a wavelength of 1,200 km is 0.76, with a phase lead of the former over the latter of 470 s. Over the Barents Sea (300 m deep sea-water), these values are 0.91 and 225 s respectively. For the shorter period of 1,200 s and a characteristic wavelength of 1,000 km, the external/total field ratio over central northern Scandinavia is 0.86 with a phase lead of 22 s. In the study of Gustafsson et al. (1981), a perfect conductor at a depth of 125 km was used to describe internal contributions in an attempt to model a very strong Ps 6 event of half-width approximately 500 km. Such an approximation gave an external/total field ratio of 0.89 with, obviously, a phase difference of 0 s. Hence, for events which exhibit a dominant period, a suitable choice of the depth of a perfect conductor is satisfactory to within the accuracies of the model-fit to data observed over central northern Scandinavia. This simple approximation is certainly not valid however if the event to be modelled has a broad power spectrum or if the activity occurs on, or near to, the coasts.

In conclusion, there is certainly a large coast-effect at all the coastal stations, including those on the Gulf of Bothnia

(PIT and OUL), and there is unequivocal evidence for a large conductivity anomaly in the region of Storavan (SRV). This anomaly may be attributable to a remnant of the Svionian island arc system. A second inland anomaly, in the vicinity of stations MAT and MIE, is tentatively proposed here, it displays a polarisation sensitivity, being apparent only for northward or southward directed equivalent current flow, i.e., for a *Y*-field. A similar anomaly has previously been located in Australia (Gough et al. 1972).

*Acknowledgements.* The author is deeply grateful to Professors U. Schmucker and J. Untiedt for critically reviewing an earlier version of this manuscript and suggesting many improvements. The author also wishes to express his gratitude to the Deutsche Forschungsgemeinschaft for financial support.

## References

Alabi, A.O., Camfield, P.A., Gough, D.I.: The north American central plains conductivity anomaly. Geophys. J.R. Astron. Soc. **43**, 815–834, 1975

Bannister, J.R., Gough, D.I.: Development of a polar magnetic substorm: A two-dimensional magnetometer array study. Geophys. J.R. Astron. Soc. **51**, 75–90, 1977

Baumjohann, W., Kamide, Y.: Joint two-dimensional observations of ground magnetic and ionospheric electric fields associated with auroral zone currents. 2. Three-dimensional current flow in the morning sector during substrom recovery. J. Geomagn. Geoelectr., in press 1981

Baumjohann, W., Untiedt, J., Greenwald, R.A.: Joint two-dimensional observations of ground magnetic and ionospheric electric fields associated with auroral zone currents. 1. Three-dimensional current flows associated with a substorm-intensified eastward electrojet. J. Geophys. Res. **85**, 1963–1978, 1980

Beer, J.H. de, Gough, D.I.: Conductive structures in southernmost Africa: a magnetometer array study. Geophys. J.R. Astron. Soc. **63**, 479–495, 1980

Bendat, J.S., Piersol, A.G.: Random data: analysis and measurement procedures. New York: Wiley-Interscience 1971

Born, J., Wolf, E.: Principles of Optics. New York: MacMillan 1964

Dosso, H.W.: A review of analogue model studies of the coast effect. Phys. Earth Planet. Inter. **7**, 294–302, 1973

Fischer, G.: Electromagnetic induction effects at an ocean coast. Proc. IEEE **67**, 1050–1060, 1979

Fischer, G., Schnegg, P.-A., Usadel, K.D.: Electromagnetic response of an ocean coast model to E-polarisation induction. Geophys. J.R. Astron. Soc. **53**, 599–616, 1978

Fowler, R.A., Kotick, B.J., Elliot, R.D.: Polarisation analysis of natural and artificially induced geomagnetic micropulsations. J. Geophys. Res. **72**, 2871–2883, 1967

Frazer, M.C.: Geomagnetic sounding with arrays of magnetometers. Rev. Geophys. Space Phys. **12**, 401–420, 1974

Glaßmeier, K.-H.: Magnetometer array observations of a giant pulsation event. J. Geophys. **48**, 127–138, 1980

Goodman, N.R.: Measurement of matrix frequency response functions and multiple coherence functions. AFFDL TR 65-56, Air Force Flight Dynamics Laboratory, Wright-Patterson AFB, Ohio, February 1965

Gough, D.I.: The interpretation of magnetometer array studies. Geophys. J.R. Astron Soc. **35**, 85–98, 1973a

Gough, D.I.: The geophysical significance of geomagnetic variation anomalies. Phys. Earth Planet. Inter. **7**, 379–388, 1973b

Gough, D.I., Beer, J.H. de: Source-field bias in geomagnetic transfer functions: A case history. J. Geomagn. Geoelectr. **32**, 471–482, 1980

Gough, D.I., Lilley, F.E.M., McElhinny, M.W.: A polarisation-sensitive magnetic variation anomaly in south Australia. Nature **239**, 88–91, 1972

Gough, D.I., Reitzel, J.S.: A portable three component magnetic variometer. J. Geomagn. Geoelectr. **19**, 203–215, 1967

Gustafsson, G., Baumjohann, W., Iversen, I.: Multi-method observations and modelling of the three-dimensional currents associated with a very strong Ps 6 event. J. Geophys. **49**, 138–145, 1981

Hermance, J.F.: Processing of magnetotelluric data. Phys. Earth Planet. Inter. **7**, 349–364, 1973

Jones, A.G.: On the difference between polarisation and coherence. J. Geophys. **45**, 223–229, 1979

Jones, A.G.: Geomagnetic Induction Studies in Scandinavia-I. Determination of the inductive response function from the magnetometer array data. J. Geophys. **48**, 181–194, 1980

Jones, A.G.: On the reduction of bias in response function estimation for hand-digitised data. Geophys. J.R. Astron. Soc., in press 1981a

Jones, A.G.: Comment on "Geomagnetic Depth Sounding by Induction Arrow Representation: A Review" by G.P. Gregori and L.J. Lanzerotti, Rev. Geophys. Space Phys., in press 1981b

Jones, A.G.: On the electrical crust mantle structure in Fennoscandia: No Moho, and the Asthenosphere revealed? Geophys. J.R. Astron. Soc., in press 1981c

Küppers, F., Post, H.: A second generation Gough-Reitzel magnetometer. J. Geomagn. Geoelectr. **33**, 225–237, 1981

Küppers, F., Untiedt, J., Baumjohann, W., Lange, K., Jones, A.G.: A two-dimensional magnetometer array for ground-based observations of auroral zone electric currents during the International Magnetospheric Study (IMS). J. Geophys. **46**, 429–450, 1979

Lilley, F.E.M.: Magnetometer array studies: A review of the interpretation of observed fields. Phys. Earth Planet. Inter. **10**, 231–240, 1975

Mareschal, M.: A modelling of some effects of the source field on the Z/H ratio evaluated at sub-auroral latitudes in the period range 15 to 60 min. (Abstract) EOS, Trans. Am. Geophys. Union **61**, 1980

Meissner, R.: Fennoscandia - A short outline of its geodynamic development. GeoJournal **3.3**, 227–233, 1979

Mersmann, U., Baumjohann, W., Küppers, F., Lange, K.: Analysis of an eastward electrojet by means of upward continuation of ground-based magnetometer data. J. Geophys. **45**, 281–298, 1979

Opgenoorth, H.J., Pellinen, R.J., Maurer, H., Küppers, F.: Heikkila, W.J., Kaila, K.U., Tanskanen, P.: Ground-based observations of an onset of localised field-aligned currents during auroral breakup around magnetic midnight. J. Geophys. **48**, 101–115, 1980

Schmucker, U.: Anomalies of geomagnetic variations in the southwestern United States. Bull. Scripps Inst. Oceanogr., Univ. Calif. Press **13**, 1970

Schmucker, U.: Interpretation of induction anomalies above nonuniform surface layers. Geophysics **36**, 156–165, 1971

Schmucker, U.: Regional induction studies: a review of methods and results. Phys. Earth Planet. Inter. **7**, 365–378, 1973

Schmucker, U.: Diskussionsbeitrag zu „Über die Unterschiede zwischen verschiedenen Definitionen der Induktionspfeile", In: Protokoll über das Kolloquium „Elektromagnetische Tiefenforschung" in Berlin, 31.3.–3.4. 1980

Untiedt, J., Pellinen, R., Küppers, F., Opgenoorth, H.J., Pelster, W.D., Baumjohann, W., Ranta, H., Kangas, J., Czechowsky, P., Heikkila, W.J.: Observations of the initial development of an auroral and magnetic substorm at magnetic midnight. J. Geophys. **45**, 41–65, 1978

Received April 6, 1981; Revised version June 14, 1981
Accepted June 25, 1981